CHEMISTRY
A EUROPEAN JOURNAL

DOI: 10.1002/chem.200600363

Structure of the α-Homo-DNA:RNA Duplex and the Function of Twist and Slide To Catalogue Nucleic Acid Duplexes

Koen Nauwelaerts, Eveline Lescrinier, and Piet Herdewijn*[a]

Abstract: High-resolution NMR studies of an α-homo-DNA:RNA duplex reveal the formation of a right-handed parallel-oriented helix. It differs significantly from a standard A- or B-type helix by a small twist value (26.2°), which leads to a helical pitch of 13.7 base pairs per helical turn, a negative inclination (−1.78 Å) and a large *x* displacement (5.90 Å). The rise (3.4 Å) is similar to that found in B-DNA. The solution of this new helix structure has stimulated us to develop a mathematical and geometrical model based on slide and twist parameters to describe nucleic acid duplexes. All existing duplexes can be positioned within this landscape, which can be used to understand the helicalization process.

Keywords: α-homo-DNA · duplex · helical structures · NMR spectroscopy · RNA

Introduction

Furanose oligonucleotides in which the base moieties at the anomeric position adopt the α-position have been shown to hybridize with β-furanose oligonucleotides in a parallel way.[1,2] α-Furanose oligonucleotides targeted to the cap site of rabbit β-globin mRNA reduce protein synthesis in a dose-dependent manner.[3] α-Furanose oligonucleotides have been studied extensively for both biological and structural reasons. This is not the case for α-pyranose oligonucleotides, of which α-homo-DNA is the simplest example.[4] These oligomers, however, are interesting for structural reasons as α-homo-DNA forms parallel duplexes with RNA, which represents the first hybridization system between hexopyranose and pentofuranose nucleic acids.[4] Modelling experiments and preliminary NMR data indicate that the base moieties of α-homo-DNA, in complex with RNA, are equatorially oriented and that the base moieties of the parallel RNA strand are pseudoaxially oriented. The duplex geometry of the model is considerably different from that of the classical A- or B-type double-stranded DNA. As the modelling results suggested the formation of a new type of helix, a more elaborated high-resolution NMR study and subsequent structure calculation were undertaken.

[a] Dr. K. Nauwelaerts, Prof. Dr. E. Lescrinier, Prof. Dr. P. Herdewijn
Laboratory of Medicinal Chemistry
Rega Institute for Medical Research
Minderbroedersstraat 10, 3000 Leuven (Belgium)
Fax: (+32) 16-337-340
E-mail: Piet.Herdewijn@rega.kuleuven.be

One of the difficulties in cataloguing helix structures of nucleic acids is the selection of parameters that represent the structure in the best way. These parameters could then be used to map duplexes and, eventually, to try and predict their hybridization properties. After solving the structure of the α-homo-DNA:RNA duplex, we concluded that the contribution of twist and slide is the best way to describe the general geometry of the helix. These parameters were then used to classify existing nucleic acid duplexes of natural and non-natural origin, and to analyse their hybridisation properties.

Results

Assignment of the NMR signals of the [α(6′-TCTAAACTC-4′)/r(5′-AGAUUUGAG-3′)] duplex: High-resolution NMR studies were undertaken to investigate the structural characteristics of an α-homo-DNA:RNA duplex. The atom numbering, chemical structure and main torsion angles of the α-homo-DNA strand are defined in Figure 1.

Nonexchangeable protons in the entire duplex could be assigned starting from an anomeric to aromatic proton walk. Sequential connectivities could be achieved (Figures 2 and 3) in the RNA and in the α-homo-DNA strands of the duplex, and provided assignments for H1′, H5, H6 and H8 protons. In the RNA strand, H2 protons could be identified through NOE contacts with the H1′ nucleus of the RNA residues at the 3′ side (residue +1) and NOE contacts with an H1′ nucleus of the opposite α-homo-DNA strand (Figure 3). In the α-homo-DNA strand, H2 protons could be identified

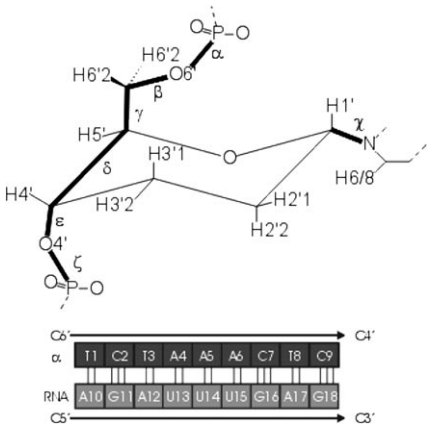

Figure 1. Top: chemical structure and main torsion angles of the α-homo-DNA nucleotides. Bottom: definition of the helix structure.

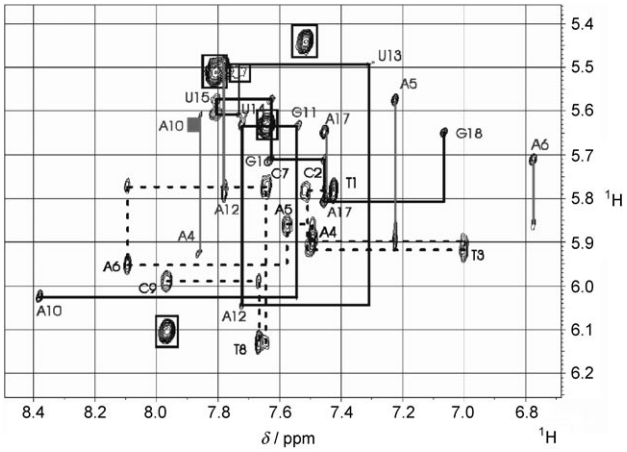

Figure 2. Nonexchangeable protons in the entire duplex could be assigned starting from an anomeric-to-aromatic proton walk. The proton walk in the RNA strand is indicated by a solid line. The walk in the α-homo-DNA strand is indicated with a dashed line. Only intra-residue peaks are labelled. Resonance signals of aromatic H2 protons with H1′ protons are indicated in grey. H5/H6 cross peaks are boxed. The H5/H6 cross peak of residue U13 is not shown as the H5 proton resonates at 5.1 ppm.

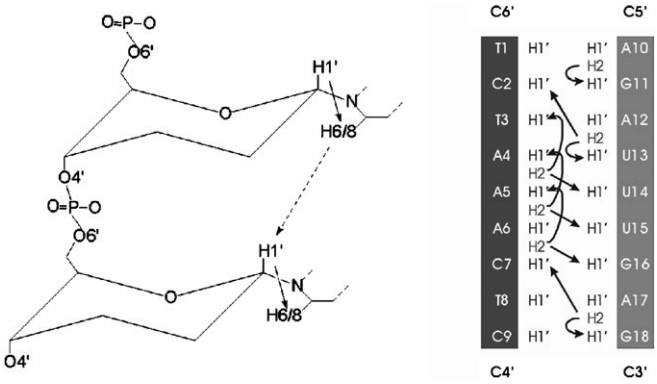

Figure 3. Anomeric-to-aromatic proton walk and connectivity of H2 and H1′ protons in the α-homo-DNA:RNA duplex.

through NOE contacts with the H1′ nucleus of the α-homo-DNA residues at the 6′ side (residue −1) and NOE contacts with an H1′ nucleus of the opposite RNA strand (Figure 3). Other protons of the spin systems were assigned from TOCSY, DQF-COSY, and NOESY spectra. All resonances were confirmed by natural abundance [^{1}H,^{13}C] HSQC. It is awkward that the carbon signals of C5 and C1′ of the α-homo-DNA residues resonate in a different offset region from the signals of the C5 and C1′ nuclei of the RNA residues. As in deoxyriboses, the altered chemical shift of C1′ is due to the absence of the 2′-OH group. A downfield shift is expected for the resonance frequency of C5 in uridine relative to C5 in cytosine due to different shielding effects in both nucleobases. This is clearly shown in Figure 4. The ^{31}P resonances were assigned from the 2D ^{1}H-detected [^{1}H,^{31}P]-correlation spectrum (HETCOR). One-dimensional imino-proton spectra recorded at various temperatures in H_2O/D_2O 9:1 showed seven sharp signals between $\delta = 12.5$ and 14.2 ppm. These signals could be assigned by means of imino-H1′ (very weak signals) and imino-to-adenine H2 cross peaks in the 2D WATERGATE-NOESY spectrum, which was confirmed by an imino-to-imino sequential proton walk (weak signals). Due to fraying at the helix ends, imino signals of G18 and T1 could not be observed.

NMR-derived restraints: After resonance assignment, all peaks in the NOESY and COSY spectra were picked and assigned. The NOESY and COSY data were subsequently translated in experimental restraints.

Distance restraints: Distance restraints were derived from NOESY spectra recorded with mixing times of 50, 100, and 150 ms by using the FELIX 97.00 software. Interproton distances were calculated based on the build-up curves. An experimental error (±20%) was used on the calculated interproton distances. The calibration of NOE cross-peak intensities was carried out against the H5–H6 cross peaks as an internal standard. In the α-homo-DNA strand this resulted in 57 inter-residue and 80 intra-residue distance restraints. In the RNA strand, 46 inter-residue and 61 intra-residue restraints could be obtained, and interstrand NOE contacts with the H2 protons of the six adenine residues resulted in 11 interstrand restraints.

Puckering restraints: Sugar puckers of the riboses in the RNA strand were inferred from the weak H1′ to H2′ ($J =<$ 2 Hz) scalar couplings and indicate N puckering of the sugar rings. In the α-homo-DNA strand, each of the anomeric H1′ protons shows a strong and a weak COSY cross peak in the high-field region between $\delta = 1.4$ and 2.5 ppm. Similar to H2′1 and H2′2 in deoxyriboses of DNA,[17] H2′1, H2′2, H3′1 and H3′2 of the nonoxygenated carbon atoms are expected to resonate at this chemical shift. The H2′ with a strong J coupling to H1′ also shows a strong geminal coupling to the H2′ that is weakly coupled to H1′ and is strongly coupled to one of the H3′ signals in the same high-field region ($\delta = 1.4$ to 2.5 ppm). The latter H3′ has a strong intra-residue NOE

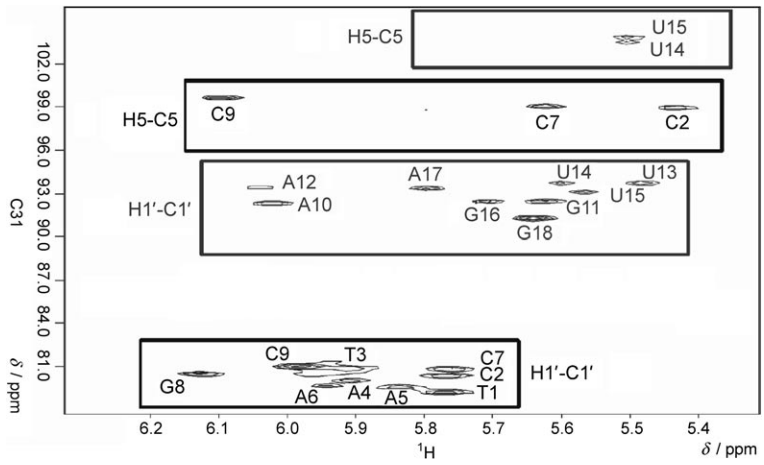

Figure 4. H5–C5 and H1′–C1′ regions of the natural abundance [^{1}H,^{13}C] HSQC. It is awkward that the carbon signals of C5 and C1′ of the α-homo-DNA residues resonate in a different offset region from the signals of the C5 and C1′ nuclei of the RNA residues.

to H1′ and a proton signal at $\delta = 4.0$–4.5 ppm, which was assigned to H4′ based on the TOCSY spectrum. None of the H4′ signals showed any strong COSY cross peaks. The data obtained on the sugar ring systems in the α-homo-DNA strand enable determination of the conformation of sugars in δ-homo(TCTAAACTC). An asymmetric six-membered ring system theoretically has two low-energy chair conformations that may interconvert through the boat and twist forms as intermediates (Figure 5). Strong ^{3}J(H,H) coupling

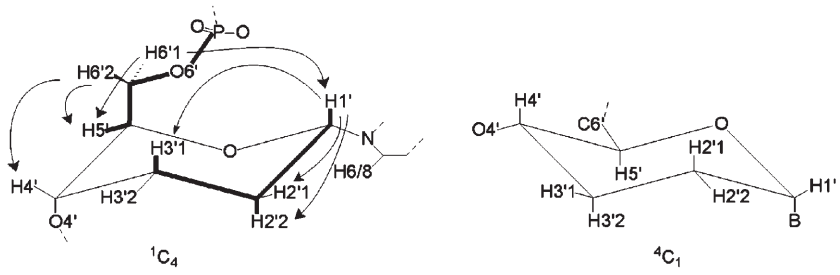

Figure 5. Chair conformations of an α-homo-DNA monomer.

(8–10 Hz) of one of the H2′ to H1′ as well as to one of the H3′ is only possible when all of these protons are predominantly in a cross-diaxial position, in which dihedral torsion angles between the considered protons are about $180 \pm 30°$. The absence of any COSY cross peaks from H4′ signals can be explained by an equatorial position of the latter which gives rise to small ^{3}J(H4′,H5′), ^{3}J(H4′,H3′1) and ^{3}J(H4′,H3′2) couplings (theoretically 2–3 Hz).[17] Only a chairlike predominant conformation of the six-membered sugar ring with the base in an equatorial position, as depicted in Figure 5 for the $^{1}C_4$ conformation, is in agreement with these experimental data. The observed intra-residue NOE contacts from H1′ to H2′1, H2′2′ and H3′1 protons confirm this as the major type of sugar conformation.

Dihedral restraints on O4′-C1′-C2′-C3′ ($-25 \pm 20°$) and C1′-C2′-C3′-C4′ ($37 \pm 20°$), to define the N-type ribose conformation, and on O5′-C1′-C2′-C3′ ($-60 \pm 20°$), C1′-C2′-C3′-C4′ ($60 \pm 20°$), C2′-C3′-C4′-C5′ ($-60 \pm 20°$), and C3′-C4′-C5′-O5′ ($60 \pm 20°$), to define the $_{1}C^{4}$ conformation of the pyranosyl ring, were used for the structure determination.

β Torsion-angle restraints: The β torsion angles of the RNA and α-homo-DNA strands were restrained to the *trans* region ($180 \pm 30°$) based on the observable four-bond J(H5′-P(n)) couplings ($J \approx 4$ Hz, Figure 5), which indicate a W-shaped conformation of the atoms P-O6′-C6′-C5′. The small and almost equal coupling constants ($J \approx 3$ Hz), which could be observed between P and H6′1/H6′2 in the α-homo-DNA strand and between P and H5′/H5″ in the RNA strand, confirm these observations.

γ Torsion-angle restraints: The small passive couplings observed in the H5′ to H5″ (RNA residue) cross peaks in the DQF-COSY spectrum, and the nicely resolved H4′-P(n) cross peak in the 2D ^{1}H-detected [^{1}H,^{31}P]-correlation spectrum, enabled us to restrain the γ torsion angles in the RNA duplex to the g+ region ($60 \pm 35°$). In the α-homo-DNA strand, close NOE contacts were observed between H6′1 and H5′, H6′2 and H5′, H6′1 and H1′, and H6′2 and H4′ (Figure 5). Analysis of proton distances in the different possible conformations around the γ torsion angle shows that this pattern of NOE contacts corresponds to a g+ conformation, which was further supported by the nicely resolved H4′-P(n) cross peak in the 2D ^{1}H-detected [^{1}H,^{31}P]-correlation spectrum. The γ torsion angle of the α-homo-DNA residues was restrained to $60 \pm 50°$.

ε Torsion-angle restraints: The ε torsion angles of the RNA residues were restrained ($230 \pm 70°$) based on steric arguments. In the δ-homo-DNA residues, no ε torsion angle constraints were applied. Other backbone angles were not restrained.

Structure calculation: To calculate the structure of the modified duplex we performed torsion angle molecular dynamics followed by a refinement of 25 selected structures using the NMR-derived restraints in X-PLOR 3.851, as described in

the Experimental Section. During the structure calculation, the experimentally determined restraints were implemented to retain interproton distances, backbone torsion angles, and sugar conformations. During calculation, the structures converged to a family of structures with similar geometry. The structure determination statistics are listed in Table 1. Inspection of the obtained structure shows that

Table 2. Backbone torsion angles and helix parameters of the α-homo-DNA:RNA duplex. Parameters highlighted in bold are diagnostic to distinguish both helix types.

	A-RNA	B-DNA	α-homo-DNA strand	RNA strand
α [°]	−50	−46	−64.3	−66.3
β [°]	−172	−147	−175.2	−171.7
γ [°]	41	36	61.0	62.2
δ [°]	**79**	**157**	**166.2**	**81.3**
ε [°]	−146	−205	−177.4	−159.3
ξ [°]	**−78**	**−96**	**−146.40**	**−72.5**
χ [°]	**−165**	**−98**	**−219**	**−167.3**
rise [Å]	**2.9**	**3.3**	**3.4 (0.5)**	
twist (local) [°]	**31.1**	**36.1**	**26.2 (2.25)**	
slide [Å]	**−1.75**	**−0.33**	**−2.8 (0.3)**	
inclination [°]	**12.0**	**2.4**	**−1.78 (8.06)**	
***x* displacement [Å]**	**4.10**	**0.8**	**5.90 (1.85)**	

Table 1. Structure determination statistics for a set of 25 structures after refinement with all experimental restraints and hydrogen bonding between base pairs.

	All restraints
total energy [kcal mol^{-1}]	210 ± 5.8
NOE violations [> 0.5 Å]	1 ± 1
dihedral violations [> 5°]	0 ± 1
RMSD from distance restraints [Å]	0.035 ± 0.005
RMSD from dihedral restraints [°]	0.210 ± 0.079
RMSD from average structure for all heavy atoms [Å]	0.633 ± 0.120

all the α-homo-DNA nucleosides occur in a $_1C^4$ conformation, all RNA residues occur in the N-puckering mode and the overall helix structure is quite different from a standard A- or B-type duplex (Figure 6).

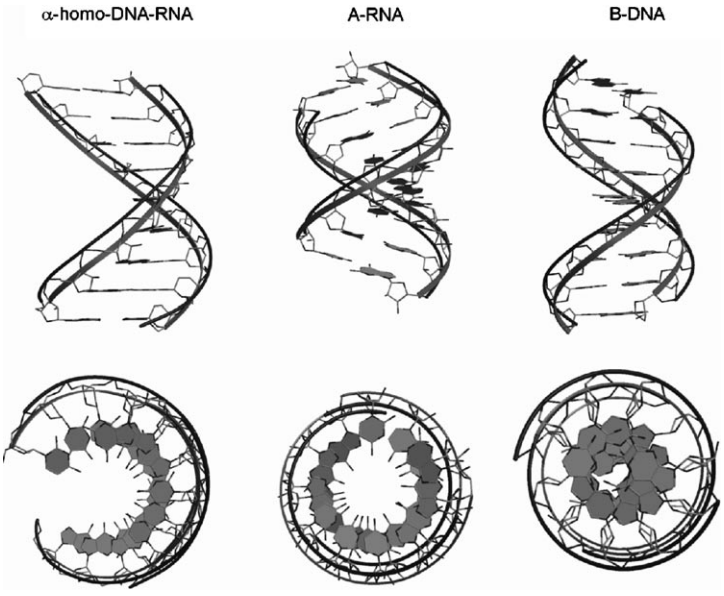

Figure 6. Visual representation of the 3D structure obtained by NMR spectroscopy. A ribbon was drawn through the C3′ atoms of each ribose moiety and the C4′ atoms of each pyranose moiety, and through the P atoms of each residue.

A comparison of helix parameters and torsion angles of the α-homo-DNA:RNA duplex under study and standard A- and B-type helices can be found in Table 2. It is clear that the helix parameters and torsion angles of the duplex are different from those of both a standard A- and B-type helix.

Discussion

The synthesis of new nucleic acid analogues in the pursuit of nucleic acid aetiology and as a tool to inhibit gene expression has led to the discovery of new nucleic acid structures. One group of synthetic nucleic acids, to which α-homo-DNA belongs, is the group that consists of nucleosides with a six-membered sugar ring and natural nucleobases, which are interconnected by a natural phosphodiester backbone. In comparison with a furanose ring, with four carbon atoms and a ring oxygen atom, the pyranose rings have an extra carbon atom in their "sugar" ring.

Here we report on the structure of the parallel-oriented [α(6′-TCTAAACTC-4′)/r(5′-AGAUUUGAG-3′)] duplex, as determined by high-resolution NMR spectroscopy and subsequent structure calculation. In the obtained structure, all the α-homo-DNA nucleosides occur in a $_1C^4$ conformation, and all RNA residues occur in the N-puckering mode. This makes α-homo-DNA the first six-membered oligonucleotide in which the base occurs in an equatorial position and both C6′ and O4′ occur in an axial position when hybridized with RNA.

The resulting helix structure is a right-handed duplex that differs significantly from a standard A- or B-type helix (Table 2). The duplex formed is characterized by a helical twist of 26.2°, leading to a helical pitch of 13.7 base pairs per helical turn. This characteristic positions the helix between the naturally occurring D,[18] C,[19] B[18] and A[18] helices with a helix pitch of 8.0, 8.5, 10.5 and 11.5 base pairs per turn, respectively, and some of the previously determined right-handed duplexes with six-membered ring sugars, such as ds HNA (type 2)[20] and double-stranded (ds) β-homo-DNA,[21] which have pitches of 15 and 30 base pairs per turn, respectively.

Unwinding of a helix (increase of helix pitch) usually leads to an increase in helical rise. The helical rise in the α-homo-DNA (3.4 Å) is, however, only slightly larger than that in standard B-DNA (3.3 Å) and still enables efficient base stacking within the helix. This observed slight increase in helical rise could contribute to a significant change in slide (B-DNA: −0.33; A-RNA: −1.75; α-homo-DNA: −2.75 Å), which allows unwinding of the helix while preventing an intolerable increase in helical rise, which would hamper base stacking (Figure 6).

In an effort to try and localize this new nucleic acid duplex in the landscape of possible helical structures (based on a previously described geometrical model),[22] we came to the conclusion that this model does not really give us insight into the way the different helical parameters are working together to obtain the observed helical structures. We also realized that slide is a parameter that may contribute to rise, which was omitted in the previous model. Therefore, we introduced a new mathematical and graphical model to represent the universe of nucleic acid helices and positioned the known nucleic acid helices in this model. The structural repertoire of double-stranded nucleic acids is, in fact, limited. Almost all natural double-stranded RNA and DNA molecules fold into an A- or B-type helical structure.

The function of twist and slide in interpretation of nucleic acid duplexes: The generation of double helices originates from several stabilizing and restraining molecular interactions. The formation of base pairs between single-stranded natural nucleic acids generates a double-stranded structure that will try to optimize stacking interactions between its consecutive base pairs. The resulting structure can be described by using several (18) helical parameters, which were divided into three sets. The first set describes the position of a base pair relative to a helix axis (helix parameters). A second set gives the position of one base relative to another within a base pair (base-pair parameters), while the third set involves the relative position of successive base pairs (step parameters). However, not all combinations of these parameters are possible. The combinations are limited by the constraints that are imposed upon the double strand by the backbone. A simple model that represents a double-stranded nucleic acid as a sequence of base pairs interconnected by static rods, which represent the backbone, can easily explain double helix formation. In a (hypothetical) fully extended double-stranded structure, base pairs are separated too much to benefit from stabilizing stacking interactions. In this case, the stacking distance is indeed equal to the interphosphate distance (5.8 Å in RNA and 7 Å in DNA due to different sugar puckering), which is much larger than the ideal stacking distance of 3–3.5 Å. To decrease this separation between base pairs and obtain an ideal stacking distance, the production of slide, shift or twist is necessary (Figure 7).

The combinations of slide, shift and twist that are used to obtain stacking in a certain double-stranded nucleic acid structure will be influenced by several factors. Some combinations are simply impossible because of steric clashes or restraints imposed by the backbone, while other combinations will be favoured due to an optimal stacking orientation, hydrogen bonding, electronic effects, hydration or other stabilizing effects.[23–26] In a double-stranded B-type DNA molecule, a large amount of twist (36.1°) and some slide (−0.33 Å) is necessary to arrive at a stacking distance of 3.3 Å (inter-phosphate distance = 7 Å). In double-stranded A-type RNA, in which the inter-phosphate distance is smaller, a smaller amount of twist (31.1°) but a larger amount of slide (−1.75 Å) is obtained to arrive at a stacking distance of 2.9 Å. Shift only accounts for a very limited amount of stacking distance reduction in both molecules. This finding can be explained by the observation that the creation of shift significantly decreases the stacking surface. As a result of the negligible effect of shift, attention will be mainly focused on the effects of slide and twist.

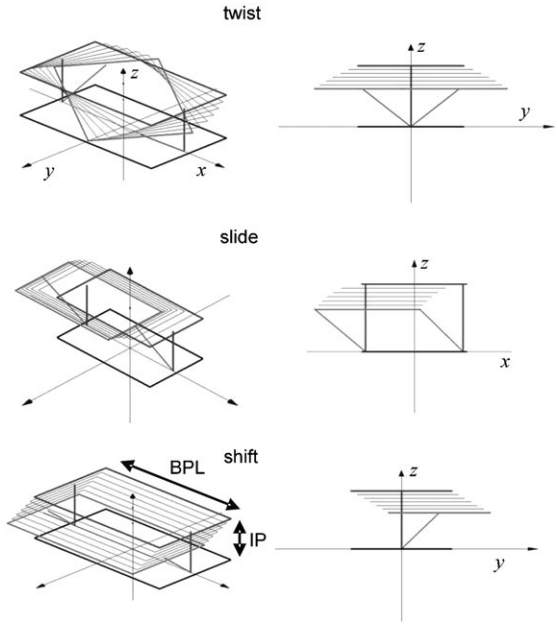

Figure 7. A simple model which represents a dinucleotide as two base pairs interconnected by static rods. To decrease the separation between these base pairs and obtain an ideal stacking distance, the production of slide, shift or twist is necessary. The initial position of the upper plane is indicated in dark grey. The position of the upper plane after slide, shift or twist is indicated in light grey. The middle of the lower plane is chosen as the origin of the axes. BPL = base-pair length; IP = initial stacking distance.

The possible combinations of slide and twist necessary to obtain a favourable stacking distance can be calculated. These combinations depend on the interphosphate distance, the exact resulting stacking distance and the length of the base pairs (C1′–C1′ distance). Figure 8 shows the combinations for molecules with an interphosphate distance between 5.5 and 7.5 Å and a base pair length of 10.7 Å, which lead to a stacking distance of 2.8–3.4 Å. Combinations that are situated between the red and green lines are favourable. Molecules with a higher inter-phosphate distance or with a lower resulting stacking distance will be situated close to the red

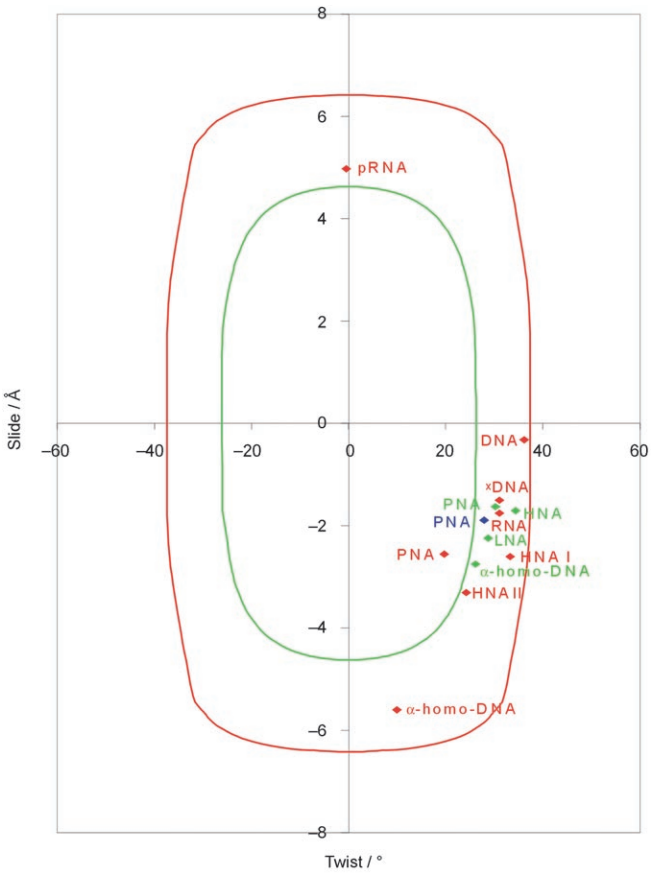

Figure 8. Combinations of slide and twist for duplexes with an interphosphate distance between 5.5 and 7.5 Å and a base-pair length of 10.7 Å, which lead to a stacking distance of 2.8–3.44 Å are situated between the red and green lines. Several homoduplexes are indicated with red symbols. Heteroduplexes with RNA are indicated in green and DNA heteroduplexes are indicated in blue.

line. Molecules with a lower interphosphate distance or with a higher resulting stacking distance will be situated close to the green line. Although slide and twist are local base-pair step parameters, their influence on the overall helical structure is significant. Local twist is representative for helical twist, while shift is a major contributor to the creation of *x* displacement.

When the restraints of the backbone are altered (for example by the introduction of a modified phosphodiester linkage or sugar residue in the backbone) or when the base-pair geometry is changed, it can be expected that other combinations of twist and slide will be found that will lead to a sufficient reduction of rise to enable base-stacking interactions. Here we analyse the structure of the available nucleic acid duplexes based on these parameters.

The structures of several double-stranded, modified oligonucleotides (ds pRNA, ds xDNA, ds PNA, ds HNA and ds β-homo-DNA) were determined by NMR and X-ray diffraction techniques. As is shown in Figure 8 and Table 3, most of these duplexes fold into helices that significantly differ from the standard A (ds RNA) and B (ds DNA) types of helix (homoduplexes are indicated in red). Notably, all of

Table 3. Parameters describing several modified homo- and heteroduplexes. Methods, local slide and local twist are listed.

	Homoduplexes					
	β-homo-DNA	pRNA	HNA I	HNA II	xDNA	PNA
method	NMR	NMR	X-ray	X-ray	NMR	X-ray
slide [Å]	−5.6	4.9	−2.6	−3.3	−1.5	−2.5
twist [°]	10.0	−0.5	33.2	24.2	31.0	19.7

	Heteroduplexes				
		RNA			DNA
	α-homo-DNA	HNA	PNA	LNA	PNA
method	NMR	NMR	NMR	NMR	NMR
slide [Å]	−2.8	−1.7	−1.6	−2.2	−1.9
twist [°]	26.1	34.4	30.3	28.8	28.0

the double-stranded molecules containing a phosphodiester linkage show combinations of twist and slide that fall into the favourable region. Only ds PNA, with an *N*-(2-aminoethyl)glycine polyamide backbone, shows a combination that seems to be unfavourable. This finding, however, can be explained by the nature of the backbone, which can obtain a rather short conformation compared to the other backbones. In a fully extended, nonhelical ds PNA molecule, base pairs would only be separated by a distance of 4.9 Å (5.8 Å in RNA and 7 Å in DNA). In this case, less twist and slide is necessary to reduce rise to a favourable distance.

The molecules for which the structures differ most significantly from the naturally occurring helices are ds β-homo-DNA[27] and ds pRNA[28–31] (Figure 9). As the backbone structure of these molecules prevents them from inducing sufficient twist, these molecules do not occur as a helical molecule. To reduce their twist to a favourable stacking distance, they are obliged to induce a large amount of twist.

The analysis of ds HNA crystal structures[20] revealed the existence of two antiparallel, right-handed Watson–Crick base-pairing double helices (types I and II in Figure 9), of which type II differs most significantly from an A- or B-type helix.

The structure of a ds xDNA molecule is very similar to that of B-DNA in many aspects[32] (Figure 10). However, because of the size expansion of the bases, the duplex diameter (as measured by the P–P interstrand distance) is increased by 3.0 Å. Moreover, the xDNA has two more base pairs per turn than B-DNA. This is primarily a result of reduced helix twist in xDNA, which is 31°, on average, as compared with 36° in B-DNA. This finding can be explained by the fact that an increase in base-pair length reduces the twist needed to arrive at a satisfactory stacking distance (see Figure 11).

The crystal structure of the right-handed PNA duplex[33–35] showed helical parameters significantly different from those of canonical DNA or RNA helical forms, thus defining a type of helix, named the P-helix (Figure 10). Some of the modified oligonucleotides are also able to form heteroduplexes with RNA (indicated in green in Figure 8) or DNA (indicated in blue in Figure 8).

Solution structures of heteroduplexes of RNA with HNA[36,37] and PNA,[38–40] determined by high-resolution NMR spectroscopy, show helix geometries which are similar

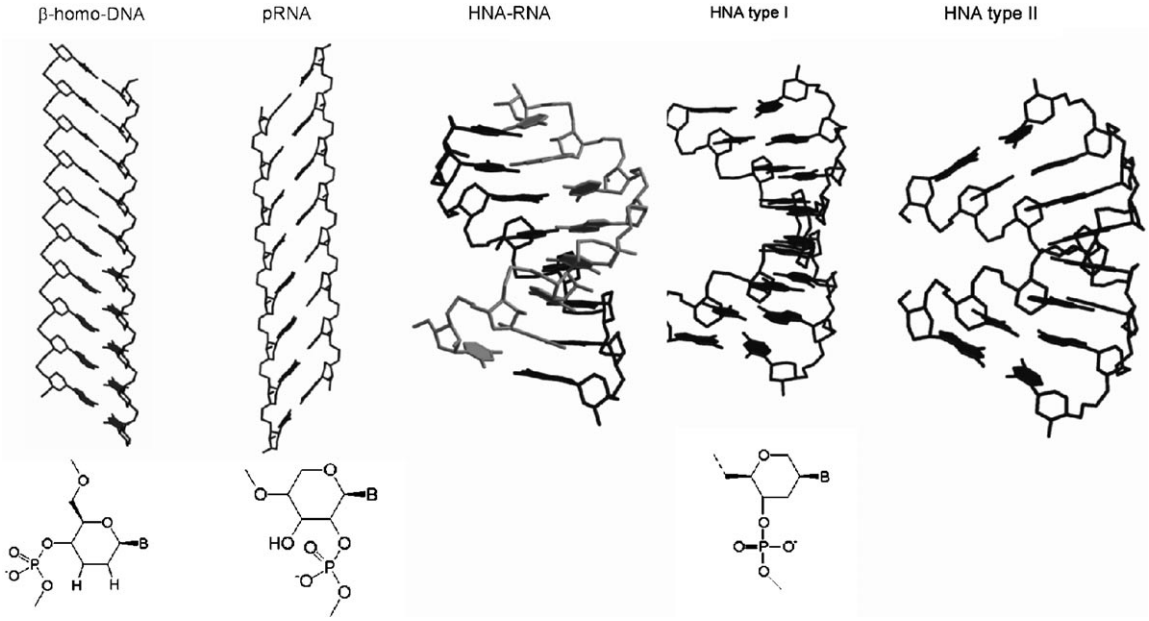

Figure 9. Comparison of β-homo-DNA, pRNA, HNA and HNA:RNA duplexes. The structures of the building blocks are represented at the bottom.

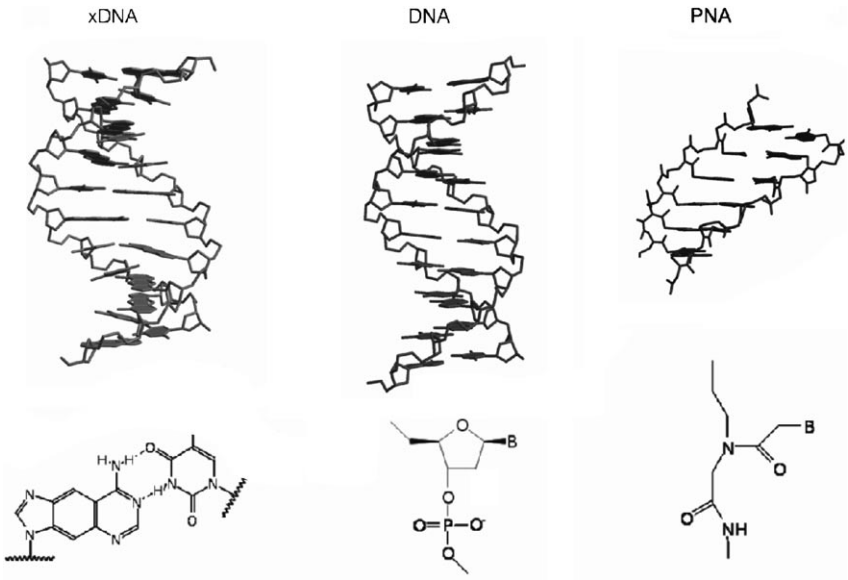

Figure 10. Comparison of xDNA, DNA and PNA duplexes. The structures of the building blocks are represented at the bottom.

to those of a standard A-type helix. These results show that HNA and PNA, for which the homoduplexes occur as helices completely different from the A type, are able to adapt their conformation to an A-type helix when hybridised with RNA.

It is not, however, true that a modified oligonucleotide has to be able to form an A-type helix to succeed in base pairing with RNA. RNA shows a certain plasticity, which enables the molecule to adapt its conformation to that of a modified oligonucleotide.[41] The solution structure of an LNA–RNA duplex,[42] determined by high-resolution NMR spectroscopy, shows that this duplex is characterized by a smaller local twist (28.7°) and larger slide (−2.24 Å) than A-type RNA.

Compared to RNA, DNA shows an even larger potential for adapting its structure to other oligonucleotides. When DNA is hybridised with PNA,[43] a new helix type, differing significantly from the standard A-, B-type helix, is formed. Furthermore, the plasticity of DNA is evident from the polymorphism of ds DNA, which can adopt an A- and B-type helix structure, and from the formation of an H-type helix when hybridized with RNA.

It is also noteworthy that no duplexes are formed between RNA or DNA and β-homo-DNA or p-RNA. As can be seen in Figure 8, the homoduplexes of these molecules differ significantly. Apparently p-RNA and β-homo-DNA are unable to adapt themselves to a possible structure of RNA or DNA.

Experimental Section

NMR sample preparation: The synthesis of the oligonucleotides was described previously.[4] The duplex used for the NMR experiments [α(6′-

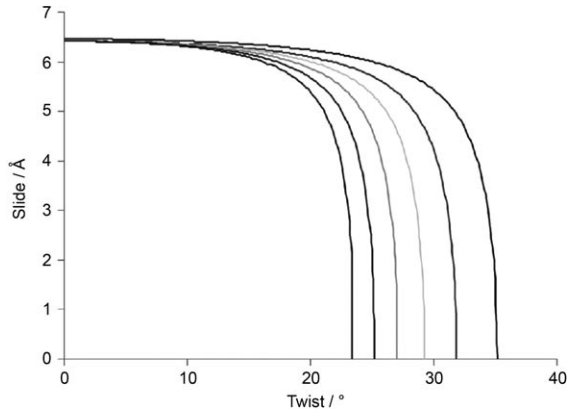

Figure 11. An increase in base-pair length reduces the twist needed to arrive at a satisfactory stacking distance. Favourable combinations of twist and slide for different base-pair lengths are shown. From left to right BPL: 15.7, 14.7, 13.7, 12.7, 11.7 and 10.7 Å.

TCTAAACTC-4′)/r(5′-AGAUUUGAG-3′)] was obtained by titrating an RNA solution r(5′-AGAUUUGAG-3′) with the complementary α-homo-DNA sequence α(6′-TCTAAACTC-4′). The degree of complex formation was monitored by one-dimensional NMR spectroscopy of nonexchangeable base protons and anomeric protons. After titration, the pD of the sample was adjusted to 7.2. The sample was lyophilized and redissolved in D_2O (0.25 mL), which resulted in a concentration of 2.4 mM of the duplex. The solution was briefly heated to 80 °C and slowly cooled to room temperature to promote duplex formation. For spectra in H_2O, the sample was again lyophilized and dissolved in H_2O/D_2O (9:1, 0.25 mL).

NMR spectroscopy: Natural abundance [^{1}H,^{13}C] HSQC (HSQC = heteronuclear single quantum correlation) and NOESY spectra in D_2O were recorded on a Bruker DRX600 spectrometer equipped with a triple-resonance cryoprobe and pulsed field gradients (EMBL Heidelberg, Germany). Other spectra were measured with our "in house" Varian Unity 500 spectrometer by using a 3 mm HCPzgrd probe. Unless stated differently, spectra were recorded at 22 °C. The spectra were processed by using the FELIX 97.00 software package (Biosym Technologies, San Diego, VA, Accelrys) running on a Silicon Graphics O2 R10000 workstation (IRIX version 6.3).

The 1D spectra in H_2O were recorded by using a jump-return pulse as the observation pulse.[5] The 2D NOESY spectrum in H_2O (mixing time 200 ms, at 5 °C) was recorded by using WATERGATE water suppression[6] with a sweep width of 10000 Hz in both dimensions, 64 scans, 2048 data points in $t2$ and 512 FIDs (FIDs = free induction decays) in $t1$. The data were apodised with a shifted sine-bell square function in both dimensions and processed to a 2×1 K matrix.

The 2D DQF-COSY (DQF = double-quantum filter),[7] TOCSY[8] and NOESY[9] spectra in D_2O were recorded with a sweep width of 4200 Hz in both dimensions. The DQF-COSY spectrum consisted of 4096 data points in $t2$ and 512 increments in $t1$. The data were apodised with a shifted sine-bell square function in both dimensions and processed to a 4×1 K matrix. Both ^{31}P-decoupled (on resonance, continuous decoupling) and ^{31}P-coupled spectra were recorded under the same conditions. For the TOCSY experiment, a clean MLEV17[10] version was used, with a low-power 90° pulse of 18.2 ms and the delay set to 47.3 ms. The total TOCSY mixing time was set to 50 ms. The spectrum was acquired with 32 scans, 2048 data points in $t2$ and 512 FIDs in $t1$. The data were apodized with a shifted sine-bell square function in both dimensions and processed to a 2×1 K matrix. The NOESY experiments were acquired with mixing times of 50, 100, 150, 250 and 300 ms, 32 scans, 2048 data points in $t2$ and 512 increments in $t1$.

A ^{1}H,^{31}P heteronuclear correlation (HETCOR)[11] spectrum was acquired with 256 scans, 2048 data points in the proton dimension $t2$, and 256 increments in the phosphorus dimension $t1$, over sweep widths of 4200 and 1600 Hz, respectively. The data were apodized with a shifted sine-bell square function in both dimensions and processed to a 2×1 K matrix.

A natural abundance [^{1}H,^{13}C] HSQC spectrum was recorded with sensitivity enhancement and gradient coherence selection[12] by using 72 scans, 256/512 complex data points and 10000/12500 Hz spectral widths in $t1$ and $t2$, respectively.

Structure determination of the [α(6′-TCTAAACTC-4′)/r(5′-AGAUUUGAG-3′)] duplex: All structure calculations were performed with X-PLOR V3.851.[13] The topallhdg.dna and parallhdg.dna files were adapted to include the α-homo-DNA nucleotides. In the topology file, three new α-homo-DNA residues were introduced (α-A, α-T, α-C). These residues were subsequently linked together in a way comparable to the treatment of RNA and DNA in the standard X-PLOR program. The modelled structures of an α-A and α-T monomer were used to derive energy constants.

The torsion angle molecular dynamics protocol used was largely identical to that proposed for a DNA duplex.[14] A set of 100 structures was generated by torsion angle molecular dynamics, starting from two extended strands and by using NMR-derived restraints.

After the torsion angle molecular dynamics round, the majority of the structures (73%) had converged to very similar structures with similar total energies (265–378 kcal mol^{-1}) and no violations of the NOE and dihedral restraints. The 25 lowest-energy structures were used for further refinement during the "gentle molecular dynamics" round.

The final refinement started with a 20 ps constant-temperature molecular dynamics simulation at 300 K (20000 steps of 0.001 ps), and was followed by a 200-step conjugate gradient energy minimisation of the average structure of the last 10 ps of the 20 ps simulation.

An analysis of the obtained 3D structure with the computer program X3DNA[15] was used to measure torsion angles and helix parameters. Finally, some visual representations of the molecule were obtained with Bobscript 2.4.[16]

Calculation of possible combinations of slide and twist to obtain favourable stacking: When a double-stranded nucleic acid is represented as a sequence of base pairs interconnected by static rods, representing the backbone, double helix formation can be regarded as the reduction of the stacking distance of a (hypothetical) fully extended double-stranded structure to an ideal stacking distance of 3–3.5 Å by the formation of slide, shift or twist (Figure 7). In several natural and chemically modified nucleic acid duplexes, only a very limited amount of shift between consecutive bases can be observed. This is most likely caused by the large reduction of stacking surface by the induction of shift. Due to the negligible effect of shift, only the effects of slide and twist will be taken into account in the further discussion.

The reduction (r) of the stacking distance (SD) by the induction of slide (dY) and twist (Ω) can be calculated as follows [Eqs. (1) and (2)]:

$$r(dY) = \sqrt{1-\frac{dY^2}{(\mathrm{IP})^2}} \quad (1)$$

$$r(\Omega) = \sqrt{1-\frac{4(\mathrm{BPL})^2\sin^2(\Omega/2)}{(\mathrm{IP})^2}} \quad (2)$$

In these equations IP represents the initial stacking distance and BPL is the C1′–C1′ length within a base pair, representing the base-pair length.

If we assume that slide and twist can independently contribute to the reduction of the stacking distance, the total reduction of the stacking distance is given by Equation (3):

$$r(dY,\Omega) = \sqrt{\left(1-\frac{dY^2}{(\mathrm{IP})^2}\right)\left((1-\frac{4(\mathrm{BPL})^2\sin^2(\Omega/2)}{(\mathrm{IP})^2}\right)} \quad (3)$$

The assumption that slide and twist act independently is a good approximation, but it should be noted that when a combination of slide and twist is obtained, the fixed-rod model requires the induction of a certain amount of shift or the induction of a combination of roll and tilt. As shift

reduces the stacking surface significantly, it can be observed that in many cases roll and tilt are generated. Equation (3) enables calculation of the combinations of slide and twist necessary to obtain a favourable stacking distance.

Conclusion

Although a complete set of 12 parameters is necessary to completely describe the 3D behaviour of a base-pair step in a duplex structure, not all combinations of these parameters are accessible. Backbone constraints limit the possible combinations of these parameters, while favourable interactions, such as stacking, drive the parameters to certain favourable combinations. Stimulated by the 3D structure of an α-homo-DNA:RNA duplex, we used a fixed-rod mathematical model to describe a nucleic acid structure and to take into account some of the constraints imposed by the backbone. The observation of rather constant stacking distances in several natural and chemically modified nucleic acids, taking into account the fixed-rod model, led to the insight that slide and twist are primarily responsible for reducing the stacking distance to a favourable distance.

Acknowledgements

The authors are indebted to K.U. Leuven (GOA) for financial support. We thank Chantal Biernaux for editorial help. K.N. is a Research Assistant of the Fund for Scientific Research, Flanders (Belgium), and E.L. is a Researcher of the Fund for Scientific Research, Flanders (Belgium).

[1] F. Morvan, B. Rayner, J. L. Imbach, M. Lee, J. A. Hartley, D. K. Chang, J. W. Lown, *Nucleic Acids Res.* **1987**, *15*, 7027–7044.
[2] N. T. Thuong, U. Asseline, V. Roig, M. Takasugi, C. Hélène, *Proc. Natl. Acad. Sci. USA* **1987**, *84*, 5129–5133.
[3] C. Boiziau, R. Kurfurst, C. Cazenave, V. Roig, N. T. Thuong, J. J. Toulmé, *Nucleic Acids Res.* **1991**, *19*, 1113–1119.
[4] M. Froeyen, E. Lescrinier, L. Kerremans, H. Rosemeyer, F. Seela, B. Verbeure, I. Lagoja, J. Rozenski, A. Van Aerschot, R. Busson, P. Herdewijn, *Chem. Eur. J.* **2001**, *7*, 5183–5194.
[5] P. Plateau, M. Gueron, *J. Am. Chem. Soc.* **1982**, *104*, 7310–7311.
[6] M. Piotto, V. Saudek, V. Sklenar, *J. Biomol. NMR* **1992**, *2*, 661–665.
[7] M. Rance, O. W. Sorensen, G. Bodenhausen, G. Wagner, R. R. Ernst, K. Wüthrich, *Biochem. Biophys. Res. Commun.* **1983**, *117*, 479–485.
[8] A. Bax, D. G. Davis, *J. Magn. Reson. Ser. A* **1985**, *65*, 355–360.
[9] J. Jeener, B. H. Meier, P. Bachmann, R. R. Ernst, *J. Chem. Phys.* **1979**, *71*, 4546–4553.
[10] C. Griesinger, G. Otting, K. Wüthrich, R. R. Ernst, *J. Am. Chem. Soc.* **1988**, *110*, 7870–7872.
[11] V. Sklenar, H. Miyashiro, G. Zon, H. T. Miles, A. Bax, *Febs Lett.* **1986**, *208*, 94–98.
[12] J. Schleucher, M. Schwendinger, M. Sattler, P. Schmidt, O. Schedletzky, S. J. Glaser, O. W. Sorensen, C. Griesinger, *J. Biomol. NMR* **1994**, *4*, 301–306.
[13] C. D. Schwieters, J. J. Kuszewski, N. Tjandra, G. M. Clore, *J. Magn. Reson.* **2003**, *160*, 65–73.
[14] E. G. Stein, L. M. Rice, A. T. Brunger, *J. Magn. Reson.* **1997**, *124*, 154–164.
[15] X. J. Lu, W. K. Olson, *Nucleic Acids Res.* **2003**, *31*, 5108–5121.
[16] R. M. Esnouf, *J. Mol. Graphics Modell.* **1997**, *15*, 132–134.
[17] S. S. Wijmenga, M. M. W. Mooren, C. W. Hilbers in *NMR of Macromolecules: A Practical Approach* (Ed.: G. C. K. Roberts), Oxford University Press, Oxford, **1993**.
[18] A. Eschenmoser, M. Dobler, *Helv. Chim. Acta* **1992**, *75*, 218–259.
[19] L. van Dam, M. H. Levitt, *J. Mol. Biol.* **2000**, *304*, 541–561.
[20] R. Declercq, A. Van Aerschot, R. J. Read, P. Herdewijn, L. van Meervelt, *J. Am. Chem. Soc.* **2002**, *124*, 928–933.
[21] G. Otting, M. Billeter, K. Wüthrich, H. J. Roth, C. Leumann, A. Eschenmoser, *Helv. Chim. Acta* **1993**, *76*, 2701–2756.
[22] E. Lescrinier, M. Froeyen, P. Herdewijn, *Nucleic Acids Res.* **2003**, *31*, 2978–2989.
[23] M. J. Packer, C. A. Hunter, *J. Am. Chem. Soc.* **2001**, *123*, 7399–7406.
[24] M. J. Packer, C. A. Hunter, *J. Mol. Biol.* **1998**, *280*, 407–420.
[25] M. J. Packer, M. P. Dauncey, C. A. Hunter, *J. Mol. Biol.* **2000**, *295*, 85–103.
[26] M. J. Packer, M. P. Dauncey, C. A. Hunter, *J. Mol. Biol.* **2000**, *295*, 71–83.
[27] G. Otting, M. Billeter, K. Wüthrich, H. J. Roth, C. Leumann, A. Eschenmoser, *Helv. Chim. Acta* **1993**, *76*, 2701–2756.
[28] K. Groebke, J. Hunziker, W. Fraser, L. Peng, U. Diederichsen, K. Zimmermann, A. Holzner, C. Leumann, A. Eschenmoser, *Helv. Chim. Acta* **1998**, *81*, 375–474.
[29] R. Micura, R. Kudick, S. Pitsch, A. Eschenmoser, *Angew. Chem.* **1999**, *111*, 715–718; *Angew. Chem. Int. Ed.* **1999**, *38*, 680–683.
[30] S. Pitsch, S. Wendeborn, B. Jaun, A. Eschenmoser, *Helv. Chim. Acta* **1993**, *76*, 2161–2183.
[31] S. Pitsch, R. Krishnamurthy, M. Bolli, S. Wendeborn, A. Holzner, M. Minton, C. Lesueur, I. Schlonvogt, B. Jaun, A. Eschenmoser, *Helv. Chim. Acta* **1995**, *78*, 1621–1635.
[32] H. B. Liu, S. R. Lynch, E. T. Kool, *J. Am. Chem. Soc.* **2004**, *126*, 6900–6905.
[33] H. Rasmussen, J. Sandholm, *Nat. Struct. Biol.* **1997**, *4*, 98–101.
[34] V. Menchise, G. De Simone, T. Tedeschi, R. Corradini, S. Sforza, R. Marchelli, D. Capasso, M. Saviano, C. Pedone, *Proc. Natl. Acad. Sci. USA* **2003**, *100*, 12021–12026.
[35] V. Menchise, G. De Simone, R. Corradini, S. Sforza, N. Sorrentino, A. Romanelli, M. Saviano, C. Pedone, *Acta Crystallogr. Sect. D* **2002**, *58*, 553–555.
[36] E. Lescrinier, R. M. Esnouf, J. Schraml, R. Busson, P. Herdewijn, *Helv. Chim. Acta* **2000**, *83*, 1291–1310.
[37] E. Lescrinier, R. Esnouf, J. Schraml, R. Busson, H. A. Heus, C. W. Hilbers, P. Herdewijn, *Chem. Biol.* **2000**, *7*, 719–731.
[38] S. Sforza, G. Haaima, R. Marchelli, P. E. Nielsen, *Eur. J. Org. Chem.* **1999**, 197–204.
[39] M. Egholm, O. Buchardt, L. Christensen, C. Behrens, S. M. Freier, D. A. Driver, R. H. Berg, S. K. Kim, B. Norden, P. E. Nielsen, *Nature* **1993**, *365*, 566–568.
[40] S. C. Brown, S. A. Thomson, J. M. Veal, D. G. Davis, *Science* **1994**, *265*, 777–780.
[41] L. Kerremans, G. Schepers, J. Rozenski, R. Busson, A. Van Aerschot, P. Herdewijn, *Org. Lett.* **2001**, *3*, 4129–4132.
[42] M. Petersen, K. Bondensgaard, J. Wengel, J. P. Jacobsen, *J. Am. Chem. Soc.* **2002** *124*, 5974–5982.
[43] V. Menchise, G. De Simone, R. Corradini, S. Sforza, N. Sorrentino, A. Romanelli, M. Saviano, C. Pedone, *Acta Crystallogr. Sect. D* **2002** *58*, 553–555.

Received: March 15, 2006
Revised: June 19, 2006
Published online: September 22, 2006

